

PCCP

Accepted Manuscript



This is an *Accepted Manuscript*, which has been through the Royal Society of Chemistry peer review process and has been accepted for publication.

Accepted Manuscripts are published online shortly after acceptance, before technical editing, formatting and proof reading. Using this free service, authors can make their results available to the community, in citable form, before we publish the edited article. We will replace this *Accepted Manuscript* with the edited and formatted *Advance Article* as soon as it is available.

You can find more information about *Accepted Manuscripts* in the [Information for Authors](#).

Please note that technical editing may introduce minor changes to the text and/or graphics, which may alter content. The journal's standard [Terms & Conditions](#) and the [Ethical guidelines](#) still apply. In no event shall the Royal Society of Chemistry be held responsible for any errors or omissions in this *Accepted Manuscript* or any consequences arising from the use of any information it contains.

Solution-Processed Bathocuproine Cathode Interfacial Layer for High-Performance Bromine-Iodine Perovskite Solar Cells

Da-Xing Yuan, Xiao-Dong Yuan, Qing-Yang Xu, Mei-Feng Xu, Xiao-Bo Shi, Zhao-Kui Wang*, and Liang-Sheng Liao*

Jiangsu Key Laboratory for Carbon-Based Functional Materials & Devices, Institute of Functional Nano & Soft Materials (FUNSOM), Soochow University, Suzhou, Jiangsu 215123, China.

*Corresponding author. Tel.: +86 512 65880927. E-mail: lsiao@suda.edu.cn zkwang@suda.edu.cn

Abstract

Perovskite film generally has rough surface morphology due to the voids between the grain domains. Smoothed interface contact between the perovskite layer and the top electrode is critical for planar perovskite solar cells. We reported high efficiency Bromine-Iodine based perovskite solar cells with a flattening cathode interface by incorporating a solution-processed bathocuproine (*s*BCP) interfacial layer at the cathode side. Compared with vacuum evaporated bathocuproine (*e*BCP), *s*BCP demonstrated excellent surface modification effect at the cathode side with very smaller charge transfer resistance. Accordingly, high fill factor exceeding 85% and power conversion efficiency exceeding 13% in $\text{CH}_3\text{NH}_3\text{PbI}_{3-x}\text{Br}_x$ based perovskite solar cells were achieved. Largely improved fill factor was attributed to the smooth film morphology and full surface coverage of perovskite films modified by the solution-processed BCP layer.

Introduction

Since the expensive manufacturing process of crystalline silicon solar cells, many efforts have been applied to develop novel solar cells. Organic solar cell (OSCs) and dye sensitized solar cells (DSSCs) are thought to be ideal candidates. Through over 20 years' efforts, their power conversion efficiencies (PCE) are still keeping as $\sim 10\%$,¹⁻⁶ which is far less than the industrial requirement. Recently, a brand new photovoltaic device known as organic-inorganic halide perovskite solar cells (PSCs) draws much attention by its rapid improvement in PCE.⁷ The amazing performance is originated from the superior optical and electrical properties of perovskite materials, such as direct optical bandgap with broad light absorption,⁸ longer carrier diffusion length,⁹⁻¹¹ low exciton binding energy^{12,13} and higher charge carrier mobilities.¹⁴ The pioneering work of employing perovskite as the light harvest by Miyasaka and co-workers in 2009 demonstrated a PCE of 3.8%.⁸ Two years later, PCE was increased to 6.5% by Park *et al.*¹⁵ Nevertheless, the device showed poor stability due to the dissolution of perovskite in liquid electrolyte. When a solid-state hole conductor small molecule of 2,2',7,7'-tetrakis(N, N -di-p-methoxyphenylamine)-9, 9'-spirobifluorene (Spiro-OMeTAD) was used as a hole transport layer, both stability and performance were improved dramatically.¹⁶ Many techniques has been utilized to improved device performance, such as introducing new methods to fabricate the perovskite layer,^{10, 17-23} controlling the annealing process,²⁴⁻²⁹ adding additives into the perovskite precursor,³¹⁻³³ compositional engineering,^{34,35} interface engineering^{31,36-45} and so on. Presently, a certified PCE above 20% have been approached.³⁰

Noticeably, most high efficiency perovskite solar cells are based on $\text{CH}_3\text{NH}_3\text{PbI}_3$ or $\text{CH}_3\text{NH}_3\text{PbI}_{3-x}\text{Cl}_x$ perovskites.^{10, 22, 26, 38, 46} Their energy band gaps are not suitable for tandem devices when integrating them with copper indium gallium selenide (CIGS) or other kind of solar cells. Recently, $\text{MAPbI}_{3-x}\text{Br}_x$ -based perovskite solar cells have drawn much attention owing to their variable energy band gap by adjusting the bromide-iodide

ratio.⁴⁷ Nevertheless, few studies on MAPbI_{3-x}Br_x system based perovskite solar cells were reported. As examples, Seok *et al.* reported meso-structured perovskite solar cells with a PCE of 12.3% by utilizing traditional one-step spin-coating method for MAPbI_{3-x}Br_x deposition.⁴⁷ Huang *et al.* achieved a 13.1% PCE in MAPbI_{3-x}Br_x-based planar perovskite solar cells by using two-step spin-coating method with solvent annealing process.⁴⁸ In planar structure PSCs, electrode interfacial layer plays very important role in the carrier behavior. For example, thermal vapor deposited LiF, bathocuproine (BCP), and fullerene (C₆₀) have been used as the cathode interfacial layer in planar structure PSCs.⁴⁸⁻⁵² Crystalline perovskite films general has rough surface morphology due to the voids between the crystals. Therefore, thermal vapor deposited interfacial layer is considered to have no positive effect on desired smooth interface between the perovskite and the electrode. In this work, we introduced a solution-processed BCP (*s*BCP) as the cathode interfacial layer in MAPbI_{3-x}Br_x perovskite solar cells. *s*BCP demonstrated excellent surface modification effect with a smoothed interface at the cathode side, which resulted in a high fill factor exceeding 85%, an average fill factor over 81% and champion PCE exceeding 13% in MAPb(I_{1-x}Br_x)₃ perovskite solar cells.

Experimental

Materials

Poly(3,4-ethylenedioxythiophene):poly(p-styrene sulfonate) (PEDOT:PSS, Clevious AI 4083) was bought from Heraeus (Germany). [6, 6]-phenyl-C60-butyric acid methyl ester (PC₆₀BM) was produced by Nichem Fine Technology Co. Ltd. (Taiwan). BCP was provided by Luminescence Technology Crop. (Taiwan). All the other chemicals were purchased from Alfa Aesar or Sigma–Aldrich and used as received without further purification. Methylammonium iodide (MAI) and Methylammonium bromide (MABr) were synthesized via the reported methods,⁴⁷ respectively. The MAPbI₃ solution of 40 wt% and MAPbBr₃ solution of 30 wt% were prepared by mixing PbI₂ and PbBr₂ powders with MAI and MABr separately with a molar ratio of 1:1. After stoichiometric

mixing of the prepared MAPbI₃ and MAPbBr₃ solutions, the desired MAPb(I_{1-x}Br_x)₃ solution was obtained. The concentration of PC₆₀BM solution was 20 mg/ml in chlorobenzene and BCP solution (0.5mg/ml) was prepared in anhydrous ethanol. All the precursor solutions were made at room temperature with stirring.

Device Fabrication

All devices were fabricated on precleaned ITO-coated glass substrates. After ultraviolet ozone treatment for 15 min, PEDOT:PSS solution was spin-coated onto the ITO surface at 4500 rpm for 40 s and then annealed at 140 °C for 15 min in air. Then, the substrates were moved into the glovebox. The MAPb(I_{1-x}Br_x)₃ perovskite layer was fabricated by fast deposition crystallization procedure and then anneal at 100 °C for 15 min. After that, PC₆₀BM and BCP was spin-coated on perovskite layer at 2000 rpm and 4000 rpm, respectively, without further annealing. Finally, a 100 nm Ag was evaporated by thermal evaporation system through a shadow mask to define the active area of the devices (0.0725 cm²). To fabricate electron-dominated devices of ITO/TiO₂/MAPbI_{2.4}Br_{0.6}/PCBM/BCP/Ag, TiO₂ was spin-coated on pre-cleaned ITO substrate at 3000rpm/40s then annealed at 150 °C for 2h. BCP was fabricated either spin-coated at 4000rpm/30s without annealing or evaporated in thermal evaporation system at 3 × 10⁻⁶ torr with an evaporation rate of 0.4 Å/s. The other layers are the same with solar cell fabrication conditions.

Measurements and Characterization

Current density-voltage (*J-V*) characteristics of perovskite solar cells under 1 Sun illumination were measured in air using a programmable Keithley 2400 source meter under AM1.5G solar irradiation at 100 mW/cm² (Newport, Class AAA solar simulator, 94023A-U). The light intensity was calibrated by a certified Oriol Reference Cell (91150 V) and verified with an NREL calibrated Hamamatsu S1787-04 diode. The EQE was performed using a certified IPCE instrument (Zolix Instruments, Inc., Solar Cell Scan 100). The ultraviolet-visible spectroscopy (UV-vis) spectra were recorded on a PerkinElmer model Lambda 750

instrument. XRD measurement was conducted using a PANalytical (Empyrean) apparatus. AFM images were obtained to evaluate the surface morphology (Veeco Multimode V instrument). SEM images were obtained from a field emission scanning electron microscope (FEI Quanta 200). Impedance spectroscopy (IS) measurements were performed using a Wayne Kerr 6550B precision impedance analyzer with a 50 mV perturbation oscillation signal in a frequency range from 20 Hz to 20 MHz.

Results and Discussion

MAPb(I_{1-x}Br_x)₃ perovskite films with different bromide concentrations were fabricated by a fast deposition crystallization procedure as previously reported.²⁰ **Fig. 1a** shows the UV-vis absorption spectra of MAPb(I_{1-x}Br_x)₃ perovskite films with varied bromide ratio *x*. With increasing the bromide content in MAPb(I_{1-x}Br_x)₃, the absorption cut-off edge decreased from 800 nm to the shorter wavelength. It indicates that the energy band gap of MAPb(I_{1-x}Br_x)₃ can be changed by the compositional engineering, which agrees well with the reported results.^{47,48} **Fig. 1b** presents the X-ray diffraction patterns of MAPbI₃ and MAPbI_{2.4}Br_{0.6} on ITO/PEDOT:PSS substrates. The zoom of X-ray diffraction from 26 to 31 degree patterns of MAPb(I_{1-x}Br_x)₃ perovskite (*x*=0, 0.2, 0.3, 0.4, 0.5) is depicted in **Fig. 1c**. The main diffraction peaks of MAPbI_{2.4}Br_{0.6} shift toward higher degrees compared with the MAPbI₃ system because the gradual substitution of the larger I atoms by the smaller Br atoms can decrease the lattice spacing at some extent. Noticeably, Seok et al. reported that MAPbI_{2.4}Br_{0.6}-based devices exhibited stable performance compared with other compositions.⁴⁷ Herein, the perovskite solar cells were all fabricated based on MAPbI_{2.4}Br_{0.6} system.

MAPbI_{2.4}Br_{0.6}-based perovskite solar cells employing solution processed BCP (sBCP) as a cathode interfacial layer with the device structure of ITO/PEDOT:PSS/MAPbI_{2.4}Br_{0.6}/PC₆₀BM/sBCP/Ag (**Fig. 2a**) were fabricated. MAPbI_{2.4}Br_{0.6}-based devices without sBCP were also fabricated for comparison. The current density-voltage (*J-V*) curves of the MAPbI_{2.4}Br_{0.6} based perovskite solar cells measured under AM 1.5G solar

illumination at 100 mW/cm^2 are shown in **Fig. 2b**. Their related photovoltaic parameters are summarized in **Table 1**. Series resistance (R_s) was extrapolated from the slopes of J - V curves at the open circuit condition. The devices with and without sBCP interfacial layer showed comparable open-circuit voltage (V_{oc}) and short-circuit current density (J_{sc}). The comparable J_{sc} was illustrated by the external quantum efficiency (EQE) spectrum, as shown in supporting information (**Fig. S1**). Noticeably, the fill factor was strongly dependent on the interfacial condition of cathode side. With sBCP modification, the fill factor was improved obviously and it approached to 85.2% in the case of sBCP modification with an optimized concentration 0.5 mg/ml.

Fig. 3a shows the J - V curve of the champion device, which exhibiting a power conversion efficiency of 13.06%, J_{sc} 18.21 mA/cm^2 , V_{OC} 0.90 V, and fill factor 0.80 under 100 mW/cm^2 AM 1.5 illumination. No obvious hysteresis was observed by changing the scan direction (**Fig. S2**). A batch of 40 devices was fabricated for getting the average performance. The average PCE (PCE_{AVE}) for the reference device (without (w/o) sBCP) and the controlled (with sBCP (0.5 mg/ml)) was 10.64% and 12.39%, respectively (**Fig. 3b**). A 16.4% improvement in PCE_{AVE} is obtained by an optimized sBCP interfacial modification. **Fig. 3c** shows the J - V characteristics of the perovskite solar cells without sBCP and incorporating sBCP (0.5 mg/ml) in dark condition. The leakage current density of the controlled device is almost one order of magnitude smaller than that in the reference device. By inserting sBCP interfacial layer, the reverse dark current was lowered obviously compared with that in the reference device. The leakage current, which is usually originates from the bad interfacial contact near the active layer,^{54,55} can reflect the interface condition at some extent. The lowered dark current suggests a better interfacial modification by the sBCP. **Figure 3d** presents the histograms (40 cells) of fill factor in reference and the controlled devices. In sBCP based devices, the fill factors locate in the range of 0.78-0.85, which was improved obviously compared to the distribution of 0.67-0.76 for the reference devices. The improved fill factor is attributed to a good interface modification by the sBCP interfacial layer, which was

agreed well with the dark current measurements.

To confirm the interface modification effect of sBCP, AFM and SEM measurements to evaluate the morphology of the $\text{MAPbI}_{2.4}\text{Br}_{0.6}$ films covered by PC_{60}BM and sBCP in order. **Fig. S3 (a), (b) and (c)** shows the AFM surface images of $\text{MAPbI}_{2.4}\text{Br}_{0.6}$, $\text{MAPbI}_{2.4}\text{Br}_{0.6}/\text{PC}_{60}\text{BM}$ and $\text{MAPbI}_{2.4}\text{Br}_{0.6}/\text{PC}_{60}\text{BM}/\text{sBCP}$ film, respectively. There was a large roughness of 8.93 nm for the $\text{MAPbI}_{2.4}\text{Br}_{0.6}$ films due to the large grain size and the voids between the crystalline domains. Compared to the general $\text{MAPbI}_{3-x}\text{Cl}_x$ film, the $\text{MAPbI}_{2.4}\text{Br}_{0.6}$ film is relative smooth. However, the roughness of 8.9 nm is still high and harmful for cathode interface contact. By covering of PC_{60}BM , the roughness was significantly reduced to 2.2 nm as shown in **Fig. S3 (b)**. The roughness was further lowered to 1.7 nm after a modification by the optimized sBCP layer. **Fig. S3 (d), (e) and (f)** presents the SEM top-view images of $\text{MAPbI}_{2.4}\text{Br}_{0.6}$, $\text{MAPbI}_{2.4}\text{Br}_{0.6}/\text{PC}_{60}\text{BM}$ and $\text{MAPbI}_{2.4}\text{Br}_{0.6}/\text{PC}_{60}\text{BM}/\text{sBCP}$ film, respectively. Interconnected crystalline areas with length scale in the range of 200-500 nm, which were the main cause for the large surface roughness, were observed in the $\text{MAPbI}_{2.4}\text{Br}_{0.6}$ film (**Fig. S3 (d)**). The voids on the $\text{MAPbI}_{2.4}\text{Br}_{0.6}$ surface were filled and the surface of the $\text{MAPbI}_{2.4}\text{Br}_{0.6}$ perovskite film was covered by the PC_{60}BM spin-coating at some extent (**Fig. S3 (e)**). Further deposition of sBCP layer smoothed the $\text{MAPbI}_{2.4}\text{Br}_{0.6}/\text{PC}_{60}\text{BM}$ surface effectively (**Fig. S3 (f)**). It means that a smoothed interface between the perovskite layer and the silver cathode can be achieved by using solution-processed BCP as the interfacial layer.

The cathode modification effect of solution-processed BCP (sBCP) was further compared with that of evaporated BCP (eBCP). The modified thickness of eBCP in device was 8 nm (**Table. S1**). **Fig.4a** shows the current density-voltage ($J-V$) curves of the inverted planar $\text{MAPbI}_{2.4}\text{Br}_{0.6}$ based perovskite solar cells employing modified evaporated BCP (eBCP) and solution-processed BCP (sBCP) as cathode interfacial layers, respectively. As shown from the key parameters in **Table 2**, sBCP based device shows higher performance due to little increase of J_{sc} and obvious increase of fill factor. The little increase of J_{sc} was consistent with their EQE

spectrum (Fig. S4).

To investigate the behind nature, sBCP- and eBCP-based electron-dominant devices with the device structure of ITO/TiO₂/ MAPbI_{2.4}Br_{0.6}/PCBM/BCP/Ag were fabricated and evaluated. The related current density-voltage characteristics were measured in dark condition as shown in Fig. 4b. Obviously, sBCP-based device shows a better current-voltage properties than the eBCP-based one. When acting as an interfacial layer in practical solar cells, sBCP-based one will demonstrate a better charge extraction behavior. Impedance spectroscopy (IS) was also utilized to study the internal series resistances (R_s) of both devices. The R_s consists of the sheet resistance (R_{sheet}) of the electrodes, the charge-transfer resistance (R_{CT}) at the interfaces between the electrode and charge carrier selective layer, as well as charge carrier selective layer and perovskite layer.⁵⁶ In this study, the major difference is the R_{CT} at the interfaces between the electrode and charge carrier selective layer. Fig. 4c shows the Nyquist plots of both sBCP and eBCP based solar cells tested under applied voltage conditions approaching the V_{oc} of perovskite solar cells. From the plots, R_{CT} values of 0.98 k Ω and 0.35 k Ω were obtained for sBCP and eBCP based solar cells, respectively. Small R_{CT} indicates that a small charge transfer resistance is resulted from the superior interfacial modification effect of sBCP. Therefore, higher performance is expected from sBCP based solar cells rather than eBCP based solar cells.

Conclusions

In summary, we have demonstrated high efficiency Bromine-Iodine based perovskite solar cells with a flattening cathode interface by incorporating a solution-processed BCP interfacial layer between the PC₆₀BM and the silver top electrode. Compared with evaporated BCP, sBCP shows superior cathode modification effect by its smaller charge transfer resistance. It can smooth the MAPbI_{2.4}Br_{0.6}/PC₆₀BM surface effectively, which resulted in reduced leakage current with one order of magnitude compared to the devices without sBCP

modification layer. As a result, high fill factor exceeding 85% and power conversion efficiency exceeding 13% were achieved in $\text{CH}_3\text{NH}_3\text{PbI}_{3-x}\text{Br}_x$ based perovskite solar cells. The high-efficient $\text{MAPbI}_{3-x}\text{Br}_x$ perovskite solar cells with high fill factor presented in this work has potential to be integrated with CIGS or other kinds of solar cells for tandem devices.

ACKNOWLEDGEMENTS

We acknowledge financial support from the Natural Science Foundation of China (Nos. 61307036 and 61177016) and from the Natural Science Foundation of Jiangsu Province (No. BK20130288). This project is also funded by the Collaborative Innovation Center of Suzhou Nano Science and Technology, and by the Priority Academic Program Development of Jiangsu Higher Education Institutions (PAPD).

SUPPORTING INFORMATION

Electronic supplementary information (ESI) available. EQE spectrum of the $\text{MAPbI}_{2.4}\text{Br}_{0.6}$ based device with and without BCP. $J-V$ curve of a representative $\text{MAPbI}_{3-x}\text{Br}_x$ -based device scan under forward and reverse directions, respectively.

Reference

1. C. W. Tang, *Appl. Phys. Lett.*, 1986, **48**, 183.
2. G. Yu, J. Gao, J. C. Hummelen, F. Wudl, A. J. Heeger, *Science*, 1995, **270**, 1789-1790.
3. H. Zhou, Y. Zhang, C.-K. Mai, S. D. Collins, G. C. Bazan, T.-Q. Nguyen and A. J. Heeger, *Adv. Mater.*, 2015, **27**, 1767-1773.
4. Z. He, B. Xiao, F. Liu, H. Wu, Y. Yang, S. Xiao, C. Wang, T. P. Russell and Y. Cao, *Nature Photon.*, 2015, **9**, 174-179.
5. B. O'Regan and M. Grätzel, *Nature*, 1991, **353**, 737-740.
6. S. Mathew, A. Yella, P. Gao, R. Humphry-Baker, B. F. Curchod, N. Ashari-Astani, I. Tavernelli, U. Rothlisberger, M. K. Nazeeruddin and M. Grätzel, *Nature Chem.*, 2014, **6**, 242-247.
7. H. S. Jung and N.-G. Park, *Small*, 2015, **11**, 10-25.
8. A. Kojima, K. Teshima, Y. Shirai and T. Miyasaka, *J. Am. Chem. Soc.*, 2009, **131**, 6050-6051.
9. S. D. Stranks, G. E. Eperon, G. Grancini, C. Menelaou, M. J. Alcocer, T. Leijtens, L. M. Herz, A. Petrozza, H. J. Snaith, *Science*, 2013, **342**, 341-344.
10. W. Nie, H. Tsai, R. Asadpour, J.-C. Blancon, A. J. Neukirch, G. Gupta, J. J. Crochet, M. Chhowalla, S. Tretiak, M. A. Alam, H.-L. Wang, A. D. Mohite, *Science*, 2015, **347**, 519-522.
11. Q. Dong, Y. Fang, Y. Shao, P. Mulligan, J. Qiu, L. Cao and J. Huang, *Science*, 2015, **347**, 967-970.
12. V. D'Innocenzo, G. Grancini, M. J. Alcocer, A. R. S. Kandada, S. D. Stranks, M. M. Lee, G. Lanzani, H. J. Snaith and A. Petrozza, *Nat. Commun.*, 2014, DOI: 10.1038/ncomms4586
13. Q. Lin, A. Armin, R. C. R. Nagiri, P. L. Burnand P. Meredith, *Nat. Photon.*, 2015, **9**, 106-112.
14. C. Wehrenfennig, G. E. Eperon, M. B. Johnston, H. J. Snaith and L. M. Herz, *Adv. Mater.*, 2013, DOI: 10.1002/adma.201305172.
15. J.-H. Im, C.-R. Lee, J.-W. Lee, S.-W. Park and N.-G. Park, *Nanoscale*, 2011, **3**, 4088-4093.
16. H.-S. Kim, C.-R. Lee, J.-H. Im, K.-B. Lee, T. Moehl, A. Marchioro, S.-J. Moon, R. Humphry-Baker, J.-H. Yum, J. E. Moser, M. Grätzel and N.-G. Park, *Sci. Rep.*, 2012, **2**, 591.
17. NREL Efficiency Chart, http://www.nrel.gov/ncpv/images/efficiency_chart.jpg, accessed 08.03.2015.
18. J. Burschka, N. Pellet, S.-J. Moon, R. Humphry-Baker, P. Gao, M. K. Nazeeruddin and M. Grätzel, *Nature*, 2013, **499**, 316-319.
19. M. Liu, M. B. Johnston and H. J. Snaith, *Nature*, 2013, **501**, 395-398.
20. Q. Chen, H. Zhou, Z. Hong, S. Luo, H.-S. Duan, H.-H. Wang, Y. Liu, G. Li, and Y. Yang, *J. Am. Chem. Soc.*, 2014, **136**, 622-625.
21. M. Xiao, F. Huang, W. Huang, Y. Dkhissi, Y. Zhu, J. Etheridge, A. Gray-Weale, U. Bach, Y.-B. Cheng and L. Spiccia, *Angew. Chem. Int. Ed.*, 2014, **126**, 10056-10061.
22. Z. Xiao, C. Bi, Y. Shao, Q. Dong, Q. Wang, Y. Yuan, C. Wang, Y. Gao and J. Huang, *Energy Environ. Sci.*, 2014, **7**, 2619-2623.
23. N. J. Jeon, J. H. Noh, Y. C. Kim, W. S. Yang, S. Ryu and S. I. Seok, *Nature Mater.*, 2014, **13**, 897-903.
24. C.-W. Chen, H.-W. Kang, S.-Y. Hsiao, P.-F. Yang, K.-M. Chiang and H.-W. Lin, *Adv. Mater.*, 2014, **26**, 6647-6652.

25. G. E. Eperon, V. M. Burlakov, P. Docampo, A. Goriely and H. J. Snaith, *Adv. Funct. Mater.*, 2014, **24**, 151-157.
26. R. Kang, J.-E. Kim, J.-S. Yeo, S. Lee, Y.-J. Jeon and D.-Y. Kim, *J. Phys. Chem. C*, 2014, **118**, 26513-26520.
27. J. You, Y. Yang, Z. Hong, T.-B. Song, L. Meng, Y. Liu, C. Jiang, H. Zhou, W.-H. Chang, G. Li and Y. Yang, *Appl. Phys. Lett.*, 2014, **105**, 183902.
28. Z. Xiao, Q. Dong, C. Bi, Y. Shao, Y. Yuan and J. Huang, *Adv. Mater.*, 2014, **26**, 6503-6509.
29. Z. Ren, A. Ng, Q. Shen, H. C. Gokkaya, J. Wang, L. Yang, W.-K. Yiu, G. Bai, A. B. Djurišić, W. W. Leung, J. Hao, W. K. Chan and C. Surya, *Sci. Rep.*, 2014, **4**, 6752.
30. F. X. Xie, D. Zhang, H. Su, X. Ren, K. S. Wong, M. Grätzel and W. C. H. Choy, *ACS Nano*, 2015, **9**, 639-646.
31. P.-W. Liang, C.-Y. Liao, C.-C. Chueh, F. Zuo, S. T. Williams, X.-K. Xin, J. Lin and Alex K.-Y. Jen, *Adv. Mater.*, 2014, **26**, 3748-3754.
32. Y. Zhao and K. Zhu, *J. Phys. Chem. C*, 2014, **118**, 9412-9418.
33. Y.-J. Jeon, S. Lee, R. Kang, J.-E. Kim, J.-S. Yeo, S.-H. Lee, S.-S. Kim, J.-M. Yun and D.-Y. Kim, *Sci. Rep.*, 2014, **4**, 6953.
34. N. Pellet, P. Gao, G. Gregori, T.-Y. Yang, M. K. Nazeeruddin, J. Maier, and M. Grtzel, *Angew. Chem. Int. Ed.*, 2014, **53**, 3151-3157.
35. N. J. Jeon, J. H. Noh, W. S. Yang, Y. C. Kim, S. Ryu, J. Seo and S. II Seok, *Nature*, 2015, **517**, 476-480.
36. P. Docampo, J. M. Ball, M. Darwich, G. E. Eperon and H. J. Snaith, *Nat. Commun.*, 2013, **4**, 2761.
37. S. Bai, Z. Wu, X. Wu, Y. Jin, N. Zhao, Z. Chen, Q. Mei, X. Wang, Z. Ye, T. Song, R. Liu, S.-T Lee, B. Sun, *Nano Research*, 2014, DOI: 10.1007/s12274-014-0534-8.
38. H. Zhou, Q. Chen, G. Li, S. Luo, T. - b. Song, H. - S. Duan, Z. Hong, J. You, Y. Liu, Y. Yang, *Science*, 2014, **345**, 542-546.
39. Q. Wang, Y. Shao, Q. Dong, Z. Xiao, Y. Yuan, J. Huang, *Energy Environ. Sci.*, 2014, **7**, 2359-2365.
40. H. Zhang, H. Azimi, Y. Hou, T. Ameri, T. Przybilla, E. Spiecker, M. Kraft, U. Scherf, and C. J. Brabec, *Chem. Mater.*, 2014, **26**, 5190-5193.
41. Q. Xue, Z. Hu, J. Liu, J. Lin, C. Sun, Z. Chen, C. Duan, J. Wang, C. Liao, W. M. Lau, F. Huang, H.-L. Yip and Y. Cao, *J. Mater. Chem. A*, 2014, **2**, 19598-19603.
42. J. Min, Z.-G. Zhang, Y. Hou, C. O. R. Quiroz, T. Przybilla, C. Bronnbauer, F. Guo, K. Forberich, H. Azimi, T. Ameri, E. Spiecker, Y. Li and C. J. Brabec, *Chem. Mater.*, 2015, **27**, 227-234.
43. Z. K. Wang, M. Li, D. X. Yuan, X. B. Shi, H. Ma, L. S. Liao, *ACS Appl. Mater. Interfaces*, 2015, **7**, 9645-9651.
44. Q. Hu, J. Wu, C. Jiang, T. Liu, X. Que, R. Zhu, Q. Gong, *ACS Nano*, 2014, **8**, 10161-10167.
45. M. Qian, M. Li, X. B. Shi, H. Ma, Z. K. Wang, L. S. Liao, *J. Mater. Chem. A*, 2015, **3**, 13533-13539.
46. D. Liu and T. L. Kelly, *Nat. Photon.*, 2013, **8**, 133-138.
47. J. H. Noh, S. H. Im, J. H. Heo, T. N. Mandal and S. II Seok, *Nano Lett.*, 2013, **13**, 1764-1769.
48. C. Bi, Y. Yuan, Y. Fang and J. Huang, *Adv. Energy Mater.*, 2014, DOI: 10.1002/aenm.201401616
49. J. Seo, S. Park, Y. C. Kim, N. J. Jeon, J. H. Noh, S. C. Yoon and S. II Seok, *Energy Environ. Sci.*, 2014, **7**, 2642-2646.

50. Q. Wang, Y. Shao, Q. Dong, Z. Xiao, Y. Yuan and J. Huang, *Energy Environ. Sci.*, 2014, **7**, 2359-2365.
51. W. Yan, Y. Li, W. Sun, H. Peng, S. Ye, Z. Liu, Z. Bian and C. Huang, *RSC Adv.*, 2014, **4**, 33039-33046.
52. W. Yan, Y. Li, Y. Li, S. Ye, Z. Liu, S. Wang, Z. Bian, C. Huang, *Nano Research*, 2015, DOI: 10.1007/s12274-015-0755-5.
53. X. Liu, H. Yu, L. Yan, Q. Dong, Q. Wan, Y. Zhou, B. Song and Y. Li, *ACS Appl. Mater. Interfaces*, 2015, **7**, 6230-6237.
54. Y. Lou, Z. Wang, S. Naka, H. Okada, *Appl. Phys. Lett.*, 2011, **99**, 033305.
55. M.-F. Xu, X.-Z. Zhu, X.-B. Shi, J. Liang, Y. Jin, Z.-K. Wang and L.-S. Liao, *ACS Appl. Mater. Interfaces*, 2013, **5**, 2935-2942.
56. J.-S. Kim, W.-S. Chung, K. Kim, D. Y. Kim, K.-J. Paeng, S. M. Jo, S.-Y. Jang, *Adv. Funct. Mater.*, 2010, **20**, 3538.

Table 1. Photovoltaic parameters of the inverted planar structure MAPbI_{2.4}Br_{0.6} based perovskite solar cells with and without solution processed BCP (*s*BCP) as interfacial layer.

| Different Configurations | J_{sc} (mA/cm ²) | V_{oc} (V) | FF(%) Average | FF(%) Highest | R_s/R_{sh} ($\Omega \cdot \text{cm}^2$) | PCE(%) Average | PCE(%) Highest |
|--------------------------|-----------------------------------|-----------------|------------------|------------------|--|-------------------|-------------------|
| w/o BCP | 16.30 | 0.89 | 0.73 | 0.76 | 25.06/2812.31 | 10.64 | 10.96 |
| BCP (3 nm) 0.1 mg/ml | 15.97 | 0.89 | 0.68 | 0.70 | 29.22/1615.54 | 9.60 | 10.03 |
| BCP (5 nm) 0.5 mg/ml | 17.07 | 0.89 | 0.81 | 0.85 | 5.10/4733.15 | 12.39 | 13.06 |
| BCP (8 nm) 1.0 mg/ml | 16.13 | 0.89 | 0.76 | 0.79 | 13.70/3306.72 | 10.81 | 11.23 |

All the photovoltaic parameters are the average of a batch of twelve devices. R_s and R_{sh} were estimated from the slopes of J-V curves at the open circuit and short circuit conditions, respectively.

Table 2. Photovoltaic parameters of the inverted planar MAPbI_{2.4}Br_{0.6} based perovskite solar cells employing modified evaporated BCP (eBCP) and solution-processed BCP (sBCP) as cathode interfacial layers, respectively.

| Solar Cells | J_{sc} (mA/cm ²) | V_{oc} (V) | Fill Factor (%) | R_s ($\Omega \cdot \text{cm}^2$) | R_{sh} ($\Omega \cdot \text{cm}^2$) | PCE (%) |
|-------------|-----------------------------------|-----------------|--------------------|---|--|------------|
| eBCP | 16.15 | 0.89 | 0.75 | 20.09 | 3088.96 | 10.73 |
| sBCP | 17.07 | 0.89 | 0.81 | 5.10 | 4733.15 | 12.39 |

All the photovoltaic parameters are the average of a batch of twelve devices.

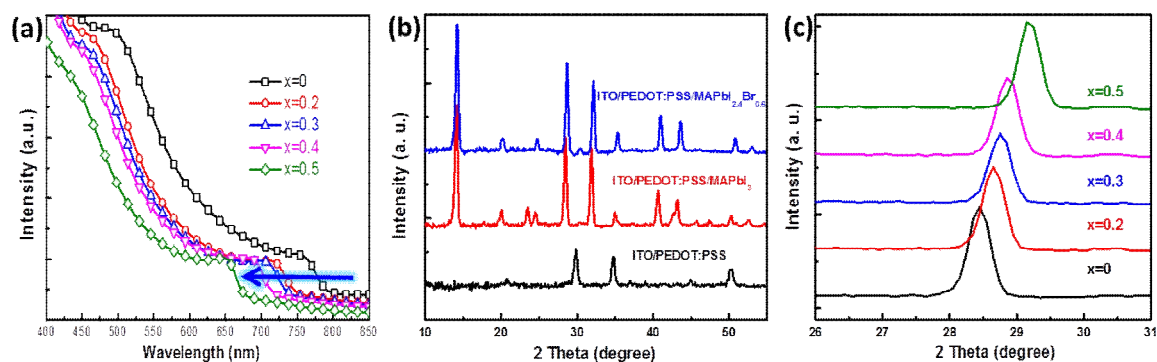


Fig. 1 (a) UV-vis absorption spectra of MAPb(I_{1-x}Br_x)₃ perovskite (x=0, 0.2, 0.3, 0.4, 0.5). (b) X-ray diffraction patterns of MAPbI₃ and MAPbI_{2.4}Br_{0.6} on ITO/PEDOT:PSS substrates. (c) The zoom of X-ray diffraction from 26 to 31 degree patterns of MAPb(I_{1-x}Br_x)₃ perovskite (x=0, 0.2, 0.3, 0.4, 0.5)

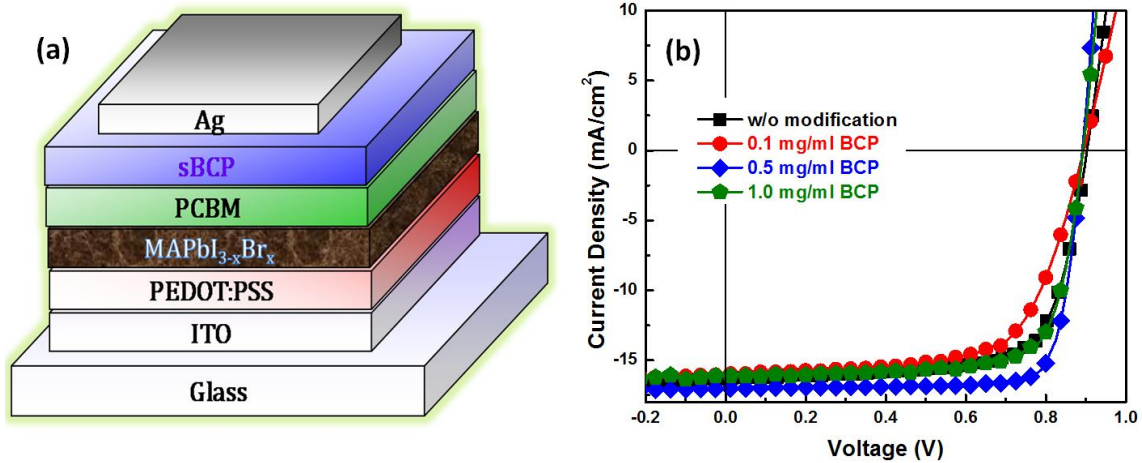


Fig. 2 (a) Device structure of the MAPbI_{2.4}Br_{0.6}-based perovskite solar cells. (b) Current density-voltage (J - V) curves of the MAPbI_{2.4}Br_{0.6} based perovskite solar cells measured under AM 1.5G solar illumination at 100 mW/cm².

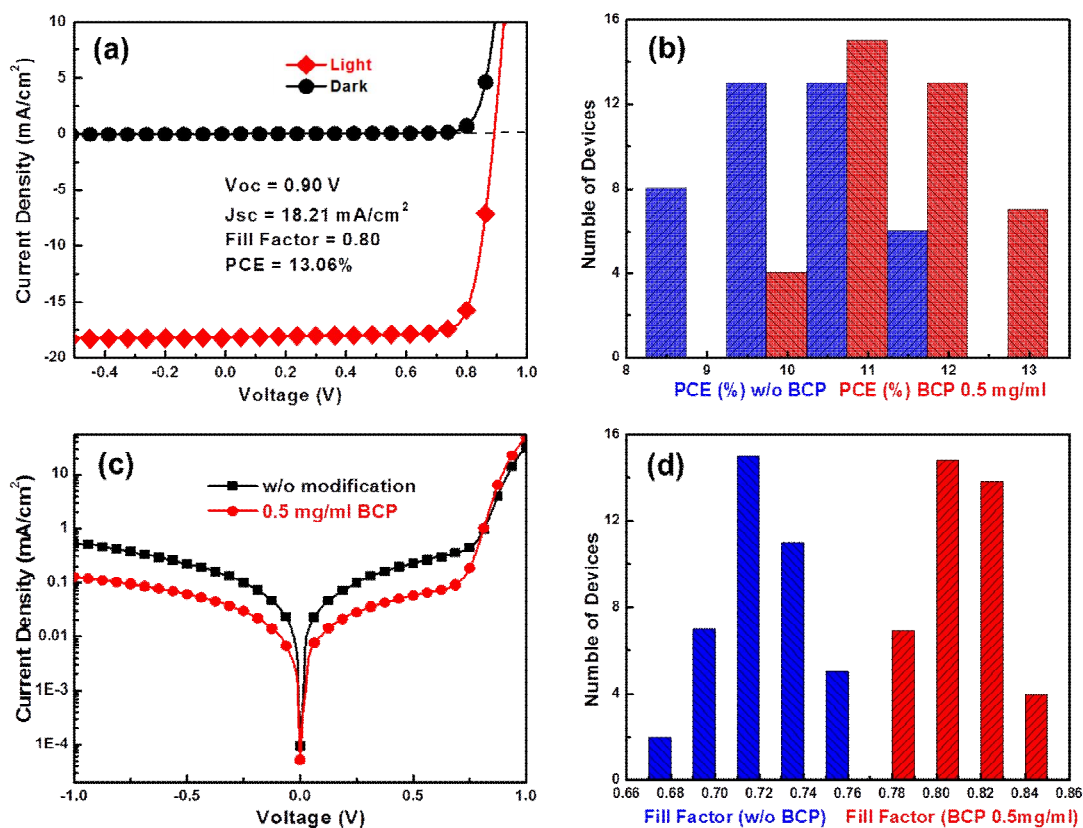


Fig. 3 (a) J - V curves of the champion device under AM 1.5G illumination of 100 mW/cm^2 (red line) and in the dark (black line). (b) Histogram of PCEs measured from perovskite solar cells (40 cells) with and without sBCP interfacial layer. (c) Dark current evaluation for perovskite solar cells with and without sBCP interfacial layer. (d) Histogram of fill factors measured from perovskite solar cells (40 cells) with and without sBCP interfacial layer.

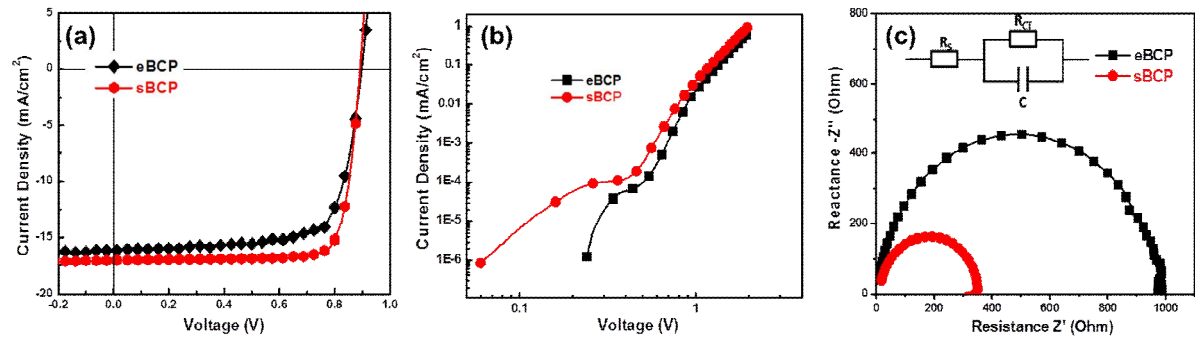


Fig. 4 (a) Current density-voltage (J-V) curves of the modified eBCP and sBCP based perovskite solar cells measured under AM 1.5G solar illumination at 100 mW/cm². (b) Current density-voltage characteristics of the sBCP and eBCP based electron only devices measured in dark condition. (c) Nyquist plots at $V \approx V_{oc}$ for eBCP and sBCP based solar cells with the device structure of ITO/PEDOT:PSS/MAPbI_{2.4}Br_{0.6}/PC₆₀BM/BCP/Ag.

Graphic Abstract

Solution-processed bathocuproine (BCP) films are prepared as the cathode interfacial layer for improving the performance of perovskite solar cells.

